

Post-print of: J. Mater. Chem. , 2010, 20, 6408-6412

DOI: 10.1039/C0JM00680G

## **TiO<sub>2</sub>–SiO<sub>2</sub> one-dimensional photonic crystals of controlled porosity by glancing angle physical vapour deposition †**

Lola González-García , Gabriel Lozano , Angel Barranco , Hernán Míguez \* and Agustín R. González-Elipe \*

Instituto de Ciencia de Materiales de Sevilla (CSIC-Univ. Sevilla), Avda. Américo Vespucio 49, 41092, Sevilla, Spain. E-mail: [hernan@icmse.csic.es](mailto:hernan@icmse.csic.es); [arge@icmse.csic.es](mailto:arge@icmse.csic.es)

Herein we present a synthetic route to attain porous one-dimensional photonic crystals of high optical quality. The method employed, based on the alternate deposition of TiO<sub>2</sub> and SiO<sub>2</sub> porous layers by glancing angle physical vapour deposition , yields a highly accessible interconnected pore network throughout the entire multilayer structure. Furthermore, it allows a strict control over the average size and density of the interstitial sites, which results in the precise tuning of the refractive index of the individual layers and thus of the optical response of the ensemble. The controlled environmental response of the multilayer is confirmed by the optical monitoring of the infiltration of liquids of different refractive index.

### **Introduction**

One-dimensional photonic crystals (1DPC) or Bragg stacks are commonly used in all branches of optics as precise frequency selective mirrors or filters. There is a wide variety of materials that can be alternated in the shape of films to achieve the periodic modulation of refractive index required to yield strongly reflecting multilayers. A preferred choice is that combining SiO<sub>2</sub> and TiO<sub>2</sub>, since these two materials present very different dielectric constants and can be grown as highly uniform thin films using a wide variety of techniques.<sup>1–7</sup> Most approaches seek to build dense phases of the deposited coatings, since performance stability under variable ambient conditions is usually desired.

Very recently, the technological potential of having optical lattices with an accessible controlled porosity has been demonstrated in different fields. Bragg reflectors with different types of pore networks have been created using metal oxide nanoparticles,<sup>8,9</sup> mesostructured thin films,<sup>10,11</sup> clays,<sup>12</sup> or macroporous alumina.<sup>13</sup> In all cases their ability to optically monitor changes in the surrounding ambient under controlled conditions has been confirmed. For instance, precise adsorption isotherms<sup>9,14</sup> or uptake kinetics<sup>15</sup> curves based on the analysis of the optical reflectance have been attained for the first time, as well as gradual, although clear and reversible, colour changes when immersed in liquids of increasing

refractive index.<sup>9–11,13</sup> They can also be devised to behave as matrices to infiltrate other materials and hence attain multifunctional structures that combine the structural photonic response with other properties such as photoconductivity, charge diffusion, light emission, or flexibility. This has recently been put into practice to build photoconducting,<sup>16</sup> lasing,<sup>17</sup> or flexible<sup>18</sup> 1DPCs, as well as to boost the efficiency of semitransparent dye sensitised solar cells.<sup>19</sup> Highly uniform and reflecting Bragg mirrors can also be realized using glancing angle physical vapour deposition (GAPVD or GLAD according to the most commonly utilized acronyms), a technique used for the fabrication of thin films with a porous columnar nanostructure, as it was shown in the seminal work by Brett and Hawkeye.<sup>20</sup> This approach was recently applied to the preparation of conducting<sup>21</sup> and photoconducting<sup>22</sup> Bragg stacks made of successively stacked layers of a single type of oxide (e.g., TiO<sub>2</sub> or indium tin oxide, ITO, respectively). In those cases, the periodic refractive index variation was achieved by modulating the porosity along the stacking direction, which leads to high optical quality materials with multiple functionalities. Their potential interest as sensing materials, since they combine the presence of accessible porosity with high optical quality, have been demonstrated by analyzing their response when exposed to different relative humidity environments.<sup>23</sup> To date, no multilayers in which the composition of each porous slab is varied has been realized by GLAD, which would provide both a wider range of refractive index contrasts and functionalities. The challenge within this approach lies in keeping the connectivity of the built-up porosity between the two different materials the alternate layers are made of.

Herein we show a synthetic route based on GLAD to attain porous 1DPCs made of layers of alternate composition that present an interconnected network of long straight pores through which the flow of species of a foreign phase is enabled, thus providing a precise response to environmental changes. We show that the technique employed allows for a precise control over both the thickness and the refractive index of the deposited films, the latter being achieved through a strict control of the pore size and density, which is in turn determined by the geometry of the deposition set-up. Photonic structures whose response can be tuned through the entire visible spectrum have been realized. Examples of the effect of variations of the ambient conditions on the optical response are shown and analyzed.

## Results and discussion

Highly uniform, mechanically stable and reflecting porous Bragg mirrors made of alternated layers of TiO<sub>2</sub> and SiO<sub>2</sub> have been realized using glancing angle physical vapour deposition (GLAD). In brief, this technique consists of the vapourization of the chosen material on a flat substrate so that the trajectory of the flux is not parallel to the substrate normal. This geometry leads to films with a characteristic tilted columnar morphology which is controlled by shadowing effects, first by the initially formed nuclei and thereafter by the growing columns.<sup>23,24</sup> A series of samples in which the porosity and the thickness of the constituent layers were varied was prepared in order to show the feasibility of the technique and to optimize the optical performance of the Bragg mirrors at different wavelength ranges. In the present work, we systematically modify both the azimuthal orientation of the substrate for the deposition of each material layer ( $\phi_{\text{TiO}_2}$ ,  $\phi_{\text{SiO}_2}$ ) and the zenithal angle formed between the normal to the substrate surface and the line connecting it to the position of the target ( $\alpha_{\text{TiO}_2}$ ,

$\alpha\text{SiO}_2$ ), as it has been described before for the preparation of multilayers of homogeneous composition.<sup>22</sup> By changing the former from one layer to the next, we achieve a uniform optical response in the long range since possible inhomogeneities along the film surface produced by the successive stacking of layers are compensated. At the same time, the zenithal angle is varied to control the features of the pore network formed, i.e., the orientation and shape of the columns defining the film microstructure. In Fig. 1 a scheme of the deposition procedure is drawn and the relevant geometrical parameters indicated. Full details on the experimental parameters employed are given in the ESI.†

In Fig. 2 we show field emission scanning electron microscopy (FESEM) images of the cross sections of  $\text{TiO}_2\text{-SiO}_2$  multilayers grown by GLAD using different azimuthal orientations of the substrate. In all cases, zenithal angles were set to  $\alpha\text{TiO}_2 = 60^\circ$  and  $\alpha\text{SiO}_2 = 85^\circ$ . Fig. 2(a) and 2(b) are secondary and backscattered electron images respectively of the same sample, in which all layers were deposited with the substrate located at a fixed azimuthal angle for the deposition of both types of materials  $\phi\text{TiO}_2 = \phi\text{SiO}_2 = 0^\circ$ . Back scattering images allow distinguishing the two components of the multilayer, being the brighter regions those corresponding to the material of higher electronic density, i.e.,  $\text{TiO}_2$ . In this case, long straight channels are created. Fig. 2(c) displays images of multilayers made employing  $\phi\text{TiO}_2 = 0^\circ$ ,  $\phi\text{SiO}_2 = 180^\circ$ . The effect of this azimuthal rotation on the pore shape and orientation can be readily seen. Finally, in Fig. 2(d), a sequence of rotations of the sort  $\phi\text{TiO}_2 = 0^\circ$ ,  $\phi\text{SiO}_2 = 90^\circ$ ,  $\phi\text{TiO}_2 = 180^\circ$ ,  $\phi\text{SiO}_2 = 270^\circ$  is used to build two stacked alternant unit cells. The pore networks of these two latter multilayers present a well controlled tortuosity and are quite homogenous in thickness and optical properties along the whole sample surface (i.e.,  $2.5 \times 2.5 \text{ cm}^2$ ).

As a consequence of the periodic variation of the refractive index in the direction perpendicular to the substrate, these coatings present coloured reflections. Under plane parallel perpendicular white light illumination, interference effects between the beams partially transmitted and reflected at each interface present in the stack may be destructive in the propagation direction (or constructive in the backwards one) for a well defined frequency range, which results in the appearance of the coloured Bragg reflection. To illustrate this, in Fig. 3 (top) we show a stripe of pictures of a series of  $\text{TiO}_2\text{-SiO}_2$  multilayers. Photographs were taken with an optical microscope operating in reflection mode and attached to a digital camera. All 1DPCs were deposited by GLAD using diverse experimental conditions, varying deposition time and both azimuthal and zenithal deposition angles for each material. The spectral position of the reflection was precisely tailored through both the refractive index and thickness (detailed in the experimental section in the ESI†) of the constituent layers, which are mainly determined by the zenithal deposition angle  $\alpha$  and the deposition time, respectively.

In the bottom part of Fig. 3, we also plot the specular reflectance spectra attained for the same series of  $\text{TiO}_2\text{-SiO}_2$  multilayers whose pictures are shown in the strip above. Each spectrum presents a well-defined maximum, which is the fingerprint of the Bragg diffraction. Secondary lobes result from the interference between beams reflected at the frontal and the rear surface of the multilayer and hence account for the finite size of the coating. Tuneability of the Bragg reflection along the whole visible spectrum is demonstrated, as well as the possibility to attain 1DPCs of good quality employing a wide range of experimental conditions.

It should be pointed out at this stage of the discussion that during fabrication of stacked structures by GLAD we found a lack of lateral uniformity when the deposition of the successive layers was done at the same azimuthal angle. Actually, the spatial analysis of the optical response reveals that the uniformity of those layered coatings made employing  $\phi_{\text{TiO}_2} = 0^\circ$ ,  $\phi_{\text{SiO}_2} = 180^\circ$  is significantly superior to those prepared with  $\phi_{\text{TiO}_2} = 0^\circ$ ,  $\phi_{\text{SiO}_2} = 0^\circ$  for the range of zenithal angles tested, namely  $60^\circ < \alpha_{\text{TiO}_2}, \alpha_{\text{SiO}_2} < 85^\circ$ . Evidence of this is provided as ESI (Fig. S1).<sup>†</sup> For this reason, and for ease of preparation, further studies were performed on samples deposited only employing  $\phi_{\text{TiO}_2} = 0^\circ$ ,  $\phi_{\text{SiO}_2} = 180^\circ$ .

We must remark that using the described methodology and the chosen individual layer thickness no significant light scattering at short wavelengths was observed. The high quality of the reflection curves in Fig. 3 and 4 and the fact that multilayered films with different positions of their reflectivity maxima present similar transmittances in the spectral zones outside that region support that light diffuse scattering in our multilayered films can be discarded (see Fig. S2 in the ESI).<sup>†</sup>

The effect of the zenithal angle,  $\alpha$ , on the porosity of the multilayers was also analyzed. In order to do so, information on the optical parameters of the different 1DPCs prepared was extracted from the fittings of the optical reflectance spectra, which were performed employing a code based on the scalar wave approximation. Full details of the calculation can be found elsewhere.<sup>25</sup> The good agreement between the experimental results and the simulations is illustrated in Fig. 4(a), in which the specular reflectance attained at normal incidence from three stacks made of 5, 7, and 9 alternate layers and their corresponding fittings are displayed. Our analysis of the optical response indicates that under the experimental conditions employed, a similar refractive index is attained for alternate layers of the same material. We can also conclude that the refractive index (porosity) of both types of layers simultaneously decreases (increases) as we increase the angle  $\alpha$ , as it is shown in Fig. 4(b) and 4(c). Although similar quantitative changes in the porosity are induced with the zenithal deposition angle in both types of layers, the effect is more significant on the refractive index of TiO<sub>2</sub> layers than on that of SiO<sub>2</sub> due to the larger value of this parameter in the dense phase of the former.

With the aim to study the accessibility of the pore network and the related environmental optical response of these materials as a function of their microstructural characteristics, we deposited two stacks displaying Bragg reflections that coincide spectrally but have porosities as different as possible. They both were made of a similar number of layers ( $L = 11$ ). In one case, we chose  $\alpha_{\text{TiO}_2} = \alpha_{\text{SiO}_2} = 60^\circ$ , which determines porosities of  $p_{\text{TiO}_2} = 31\%$  and  $p_{\text{SiO}_2} = 36\%$  and a refractive index contrast of  $n_{\text{TiO}_2}/n_{\text{SiO}_2} = 1.35$ . In another, the zenithal angles were set to  $\alpha_{\text{TiO}_2} = \alpha_{\text{SiO}_2} = 85^\circ$ , which implies that  $p_{\text{TiO}_2} = 51\%$  and  $p_{\text{SiO}_2} = 47\%$  and that  $n_{\text{TiO}_2}/n_{\text{SiO}_2} = 1.2$ . FESEM analysis of the cross sections reveal clear variations in the pore size, being much larger for the multilayer of higher porosity, as can be readily seen in Fig. 5. These results demonstrate that GLAD allows for a rational design of the voids in 1DPCs. In turn, this possibility allows us precise control of both the features of the optical response and the magnitude of its variation to ambient changes, as it will be shown next. The two 1DPCs with

different porosity were infiltrated with a series of liquids of increasing refractive index. The corresponding reflectance spectra are shown in Fig. 6(a) and 6(b). As the void network of the multilayers is filled with a higher refractive index solvent, the spectral position of the Bragg reflection linearly red-shifts, as can be observed in Fig. 6(c). In both cases, the values of the optical parameters extracted from the fittings of the spectra of the infiltrated samples doubtlessly demonstrate that the empty volume present in the original multilayer is filled up to a degree between 90% and 100%. This confirms the accessibility and good connectivity of the pores created in each type of material present in the stack. Despite the large porosity of these films, they are quite robust and mechanically stable, without any noticeable “nanocarpet effect”<sup>26</sup> after infiltration with water (see ESI Fig. S3†). As expected, the spectral displacements are more pronounced for the structure with the largest porosity. At the same time, for a given number of layers in the stack, a lower refractive index contrast yields thinner and less intense Bragg reflectance peaks.<sup>27</sup> Narrower peaks and larger shifts are desirable in order to enhance the resolution of a potential sensing device making use of this effect, but for porous 1DPCs with a limited number of layers, as it is our case, increase of resolution will always be at the expense of the intensity of the diffraction peak.

## Conclusions

We have demonstrated a synthetic route based on glancing angle physical vapour deposition to attain porous one-dimensional photonic crystals made of layers of alternate composition that present an interconnected network of pores and that can be handled without any particular precaution.<sup>28</sup> This vacuum technique is used in industry, for instance for processing ophthalmic lenses, and can be easily scaled-up for series production. We show that it allows for a precise command over both the thickness and the refractive index of the deposited films, the latter being achieved through a strict control of the porosity. We have also shown that the ease of infiltration of different species embedded within the void network yields a precise optical response to environmental changes, which can be tailored through the design of the microstructural features. We foresee that these structures will find applications in fields such as sensing, light emission or photovoltaics, as it has been recently demonstrated for other types of porous Bragg stacks.

## Acknowledgements

This work has been funded by the Ministry of Science and Innovation of Spain through grants MAT2008-02166 and MAT2007-65764, Consolider Projects (HOPE CSD2007-00007 and CSD2008-00023), and Junta de Andalucía through grants FQM-3579 and TEP2275.

## Notes and references

1. H. A. Macleod, *Thin Film Optical Filters*, Institute of Physics Publishing, London, 3rd edn, 2001.
2. K. M. Chen, A. W. Sparks, H. C. Luan, R. D. Lim, K. Wada and L. C. Kimerling, *Appl. Phys. Lett.*, 1999, 75, 3805.
3. Q. Zhang, X. Li, J. Shen, G. Wu, J. Wang and L. Chen, *Mater. Lett.*, 2000, 45, 311
4. S. Rabaste, J. Bellessa, A. Brioude, C. Bovier, J. C. Plenet, R. Brenier, O. Marty, J. Mugnier and J. Dumas, *Thin Solid Films*, 2002, 416, 242
5. R. M. Almeida and S. Portal, *Curr. Opin. Solid State Mater. Sci.*, 2003, 7, 151
6. R. M. Almeida and A. S. Rodrigues, *J. Non-Cryst. Solids*, 2003, 326–327, 405
7. P. K. Biswas, D. Kundu and D. Ganguli, *J. Mater. Sci. Lett.*, 1987, 6, 1481
8. Z. Wu, D. Lee, M. F. Rubner and R. E. Cohen, *Small*, 2007, 3, 1445
9. S. Colodrero, M. Ocana, A. R. Gonzalez-Elipé and H. Miguez, *Langmuir*, 2008, 24, 9135
10. S. Y. Choi, M. Mamak, G. von Freymann, N. Chopra and G. A. Ozin, *Nano Lett.*, 2006, 6, 2456
11. M. C. Fuertes, F. J. Lopez-Alcaraz, M. C. Marchi, H. E. Troiani, V. Luca, H. Miguez and G. J. D. A. Soler-Illia, *Adv. Funct. Mater.*, 2007, 17, 1247
12. B. V. Lotsch and G. A. Ozin, *ACS Nano*, 2008, 2, 2065
13. D. Guo, L. Fan, F. Wang, S. Huang and X. Zou, *J. Phys. Chem. C*, 2008, 112, 17952
14. M. C. Fuertes, S. Colodrero, G. Lozano, A. R. Gonzalez-Elipé, D. Grosso, C. Boissiere, C. Sanchez, G. J. D. A. Soler-Illia and H. Miguez, *J. Phys. Chem. C*, 2008, 112, 3157
15. B. V. Lotsch and G. A. Ozin, *Adv. Mater.*, 2008, 20, 4079
16. M. E. Calvo, S. Colodrero, T. C. Rojas, J. A. Anta, M. Ocana and H. Miguez, *Adv. Funct. Mater.*, 2008, 18, 2708
17. F. Scotognella, D. P. Puzzo, A. Monguzzi, D. S. Wiersma, D. Maschke, R. Tubino and G. A. Ozin, *Small*, 2009, 5, 2048
18. M. E. Calvo, O. Sanchez Sobrado, G. Lozano and H. Miguez, *J. Mater. Chem.*, 2009, 19, 3144
19. S. Colodrero, A. Mihi, L. Haggman, M. Ocana, G. Boschloo, A. Hagfeldt and H. Miguez, *Adv. Mater.*, 2009, 21, 764
20. M. J. Brett and M. M. Hawkeye, *Science*, 2008, 319, 1192

21. J. J. Steele, A. C. van Popta, M. M. Hawkeye, J. C. Sit and M. J. Brett, *Sens. Actuators, B*, 2006, 120, 213
22. M. F. Schubert, J.-Q. Xi, J. K. Kim and E. F. Schubert, *Appl. Phys. Lett.*, 2007, 90, 141115
23. J. J. Steele and M. J. Brett, *J. Mater. Sci.: Mater. Electron.*, 2007, 18, 367
24. J. R. Sánchez-Valencia, A. Borrás, A. Barranco, V. J. Rico, J. P. Espinós and A. R. González-Elipe, *Langmuir*, 2008, 24, 9460
25. G. Lozano, S. Colodrero, O. Caulier, M. E. Calvo and H. Míguez, *J. Phys. Chem. C*, 2010, 114, 3681
26. Y. Gaillard, V. J. Rico, E. Jiménez-Piqué and A. R. González-Elipe, *J. Phys. D: Appl. Phys.*, 2009, 42, 145305
27. A. Yariv, P. Yeh, "Optical Waves in Crystals", Wiley Classics Library, John Wiley & Sons Inc, Hoboken, New Jersey, ISBN 0-471-43081-1
28. J.-G. Fan, D. Dyer, G. Zhang and Y.-P. Zhao, *Nano Lett.*, 2004, 4, 2133

#### Footnote

† Electronic supplementary information (ESI) available: Experimental conditions employed to prepare the multilayers shown in this work; analysis of the spatial uniformity of the films realized with micro-optical reflectance; optical evidence of the lack of diffusely scattered light; SEM pictures demonstrating the absence of the nanocarpets effect. See DOI: 10.1039/c0jm00680g

## Figure captions

Figure 1. A scheme of the experimental set-up in which the relevant geometrical parameters are indicated.

Figure 2. Secondary, (a), (c) and (d), and backscattered, (b), electron microscopy images of cross sections of TiO<sub>2</sub>–SiO<sub>2</sub> multilayers deposited on glass by glancing angle physical vapour deposition. In all cases, zenithal deposition angles were set to  $\alpha_{\text{TiO}_2} = 60^\circ$  and  $\alpha_{\text{SiO}_2} = 85^\circ$ , while azimuthal deposition angles were: (a) and (b)  $\phi_{\text{TiO}_2} = \phi_{\text{SiO}_2} = 0^\circ$ ; (c)  $\phi_{\text{TiO}_2} = 0^\circ, \phi_{\text{SiO}_2} = 180^\circ$ ; (d) a sequence of rotations of the sort  $\phi_{\text{TiO}_2} = 0^\circ, \phi_{\text{SiO}_2} = 90^\circ, \phi_{\text{TiO}_2} = 180^\circ, \phi_{\text{SiO}_2} = 270^\circ$ .

Figure 3. Top: A strip of photographs taken with an optical microscope under normal white light illumination of different TiO<sub>2</sub>–SiO<sub>2</sub> multilayers deposited by GLAD. The details of each sample are in the ESI.† Bottom: The corresponding normal incidence specular reflectance spectra.

Figure 4. (a) Normal incidence specular reflectance spectra (—) and their corresponding fittings (---) for porous Bragg stacks deposited by GLAD as the number of layers,  $L$ , increases. (b) and (c) show the values of the refractive index and the porosity, respectively, extracted from the fittings of samples grown under different conditions, as a function of the zenithal angle. Filled triangles and open circle symbols refer to data for the TiO<sub>2</sub> and the SiO<sub>2</sub> layers, respectively.

Figure 5. Electron microscopy images of cross sections of TiO<sub>2</sub>–SiO<sub>2</sub> multilayers deposited on silicon wafer (100) by glancing angle physical vapour deposition using (a)  $\phi_{\text{TiO}_2} = 0^\circ, \phi_{\text{SiO}_2} = 180^\circ, \alpha_{\text{TiO}_2} = \alpha_{\text{SiO}_2} = 60^\circ$  and (b)  $\phi_{\text{TiO}_2} = 0^\circ, \phi_{\text{SiO}_2} = 180^\circ, \alpha_{\text{TiO}_2} = \alpha_{\text{SiO}_2} = 85^\circ$ .

Figure 6. Normal incidence specular reflectance spectra of two 1DPCs made by GLAD possessing different porosity. Results are shown for samples made employing (a)  $\phi_{\text{TiO}_2} = 0^\circ, \phi_{\text{SiO}_2} = 180^\circ, \alpha_{\text{TiO}_2} = \alpha_{\text{SiO}_2} = 60^\circ$  and (b)  $\phi_{\text{TiO}_2} = 0^\circ, \phi_{\text{SiO}_2} = 180^\circ, \alpha_{\text{TiO}_2} = \alpha_{\text{SiO}_2} = 85^\circ$ , respectively. Each curve corresponds to a different fluid filling the voids, namely, air (dark grey solid line), water (black solid line), isopropanol (black dashed line), toluene (light grey solid line), Cl-benzene (light grey dashed line). (c) A plot of the spectral position at which the maximum Bragg reflection is observed versus the refractive index of the infiltrated liquid.



Figure 1

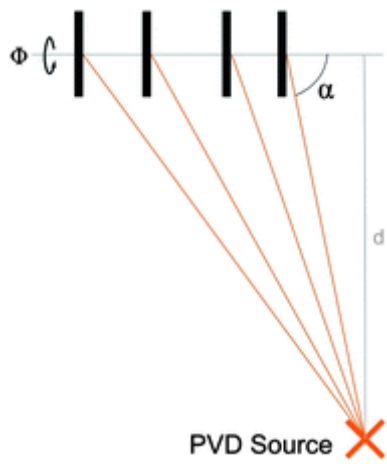


Figure 2

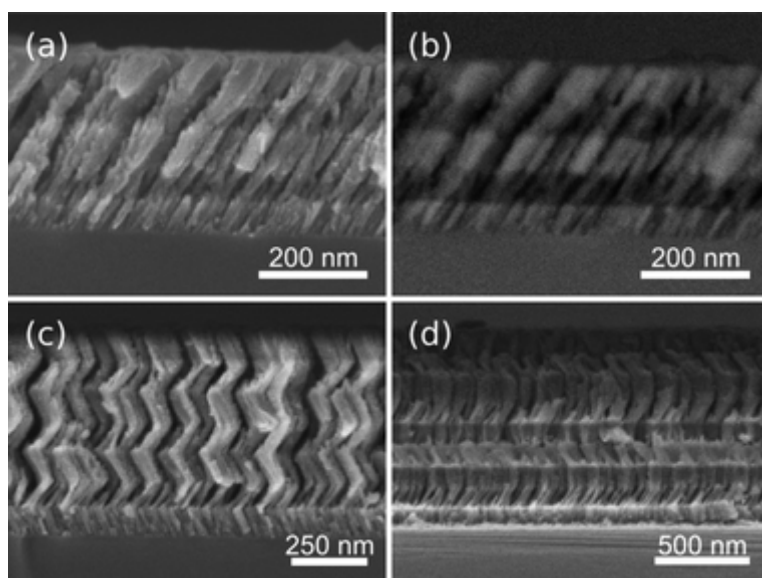


Figure 3

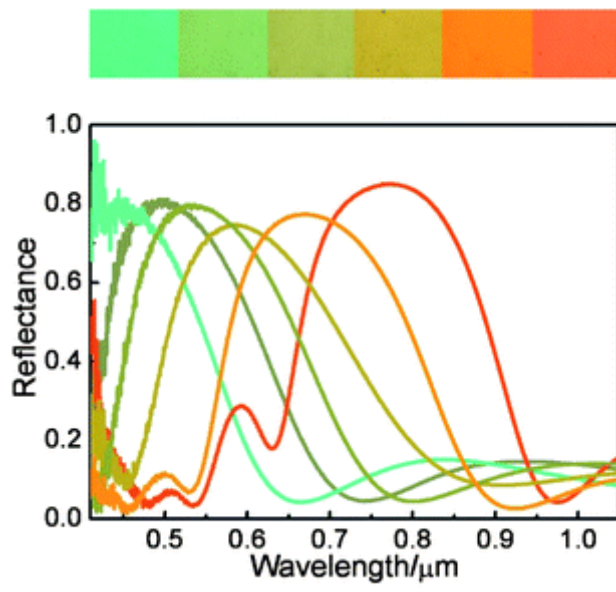


Figure 4

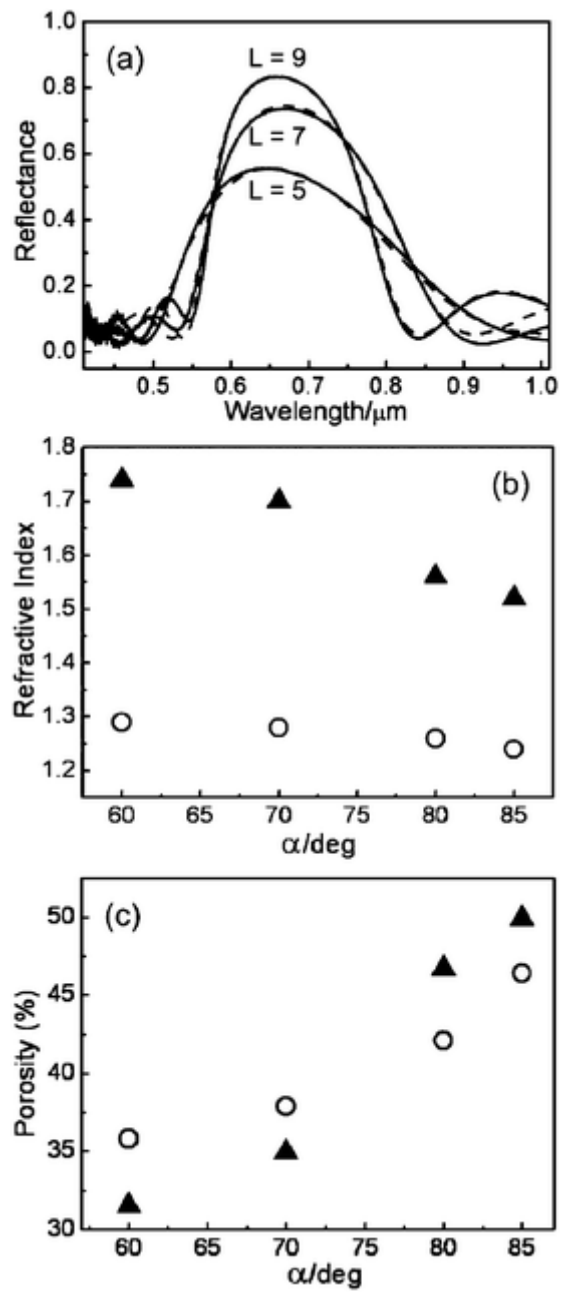


Figure 5

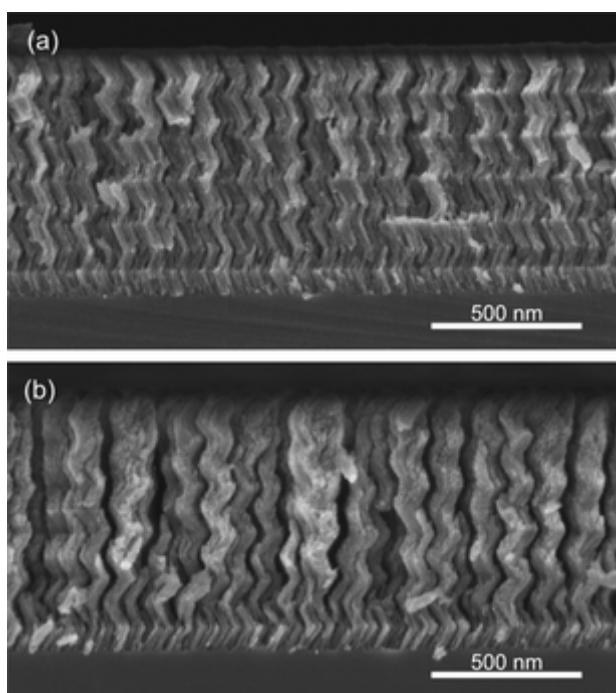


Figure 6

